Research Square

Preprints are preliminary reports that have not undergone peer review.
They should not be considered conclusive, used to inform clinical practice,
or referenced by the media as validated information.

Modeling Hepatic Fibrosis and Screening Anti-Fibrotic Compounds Based on Multi-Lineage Hepatic Organoids

Wenyue Cheng
Tianjin Institute of Pharmaceutical Research
Sen Liu
Shenyang Pharmaceutical University
Libo Wang
Tianjin Institute of Pharmaceutical Research
Zhenzhen Li
Tianjin Institute of Pharmaceutical Research
Putian Yu
Tianjin Institute of Pharmaceutical Research
Xiaolei Zhou
Tianjin Institute of Pharmaceutical Research
Tianyu Zhao
Tianjin Institute of Pharmaceutical Research
Xiaoliang Wang
Tianjin Institute of Pharmaceutical Research
Ze Wang
wangze9452@163.com

Tianjin Institute of Pharmaceutical Research

Research Article

Keywords: Liver fibrosis, HUVEC, LX-2, Organoids, Disease model, TGF-β, COL1A1, PI3K/AKT

Posted Date: September 8th, 2026

DOI: https://doi.org/10.21203/rs.3.rs-10572430/v1

License: This work is licensed under a Creative Commons Attribution 4.0 International License.
Read Full License

Additional Declarations: No competing interests reported.

Abstract

Introduction:

The liver is a vital parenchymal organ responsible for systemic synthesis, metabolism, immune modulation and substance storage to maintain body homeostasis. Chronic hepatic injury triggers progressive liver disorders that severely endanger human health. Conventional in vitro liver models fail to recapitulate native liver physiology, which hinders mechanistic research of liver fibrosis and anti-fibrotic drug discovery.

Objectives

This study aimed to construct a human multi-lineage liver organoid platform for fibrotic drug screening, and characterize the anti-fibrotic efficacy and molecular mechanism of the novel aspirin derivative AS191.

Methods

A 3D multi-human-lineage liver organoid model (3hlLOs) was built by co-culturing iPSC-derived hepatic organoids, HUVECs and LX-2 hepatic stellate cells. TGF-β was applied to induce fibrotic injury for compound screening. Cellular fibrosis phenotypes were validated in LX-2 cells, and in vivo therapeutic effects were verified using a CCl_4-induced mouse liver fibrosis model. Signaling pathway changes were detected to clarify the underlying mechanism.

Results

The established 3hlLOs successfully recapitulated fibrotic pathological features under TGF-β treatment. Screening identified AS191 as a potent anti-fibrotic candidate. AS191 suppressed TGF-β-triggered COL1A1 accumulation in vitro and relieved collagen deposition and liver dysfunction in fibrotic mice. Mechanically, AS191 downregulated profibrotic genes by inhibiting the non-canonical TGF-β/PI3K/AKT axis in hepatic fibroblasts.

Conclusion

The engineered 3hlLOs serve as a feasible and physiological platform for anti-fibrotic compound screening. AS191 exerts prominent protective effects against hepatic fibrosis via suppressing PI3K/AKT signaling, and has great potential as a therapeutic agent for fibrotic liver diseases.

1 Introduction

As the largest glandular organ in humans, the liver executes core physiological functions including metabolism, digestion, detoxification, and immune regulation[1]. Hepatic fibrosis is a common pathological precursor triggered by multiple chronic liver injuries, including viral hepatitis, alcoholic liver disease, non-alcoholic fatty liver disease, and hypoxic liver damage[2]. Fibrosis is characterized by excessive accumulation of fibrillar extracellular matrix (ECM) components, predominantly type I and type III collagen[3]. Excessive ECM deposition disrupts hepatic sinusoidal microcirculation and nutrient exchange between blood and hepatocytes, ultimately leading to irreversible hepatic dysfunction[4]. Without effective intervention, persistent liver injury drives progressive fibrosis toward cirrhosis, hepatocellular carcinoma (HCC), and even end-stage liver failure, which constitutes a major cause of liver-related mortality[5, 6]. During fibrotic progression, quiescent hepatic stellate cells (HSCs) are robustly activated into proliferative myofibroblasts (MFBs), which serve as the primary cellular source of ECM synthesis and are considered the central effector cells of hepatic fibrogenesis[7, 8].

Current clinical management of liver fibrosis mainly relies on etiological intervention, including antiviral therapy for HBV/HCV infection, lifestyle and metabolic modulation for fatty liver disease, and ursodeoxycholic acid treatment for primary biliary cholangitis[9]. However, accumulating clinical evidence indicates that eliminating pathogenic stimuli can only slow fibrotic progression but fails to reverse established hepatic scarring. In recent years, resmetirom has obtained FDA accelerated approval for NASH with fibrosis, while semaglutide and obeticholic acid are under investigation in clinical trials for liver fibrosis but have not yet received FDA approval for this indication. Additionally, the pulmonary fibrosis drugs pirfenidone and nintedanib, originally approved for idiopathic pulmonary fibrosis, are currently under investigation in early-phase clinical trials for liver fibrosis, with limited published efficacy data[10]. Nevertheless, these available drugs still exhibit limitations such as narrow indications and potential adverse effects, and effective broad-spectrum anti-fibrotic candidates remain insufficient.

Conventional anti-fibrotic drug screening heavily depends on animal models, which possess notable drawbacks. Animal modeling is time-consuming and labor-intensive, usually requiring months to establish stable fibrotic phenotypes[11, 12]. Moreover, substantial interspecies and inter-strain differences restrict the ability of animal models to recapitulate the complex and multifactorial features of human liver diseases, thereby hindering the development of precise and personalized hepatic therapeutics.

Three-dimensional (3D) liver organoid technology has emerged as a powerful platform for disease modeling, high-throughput drug screening, and toxicological evaluation[13, 14]. In this study, we constructed a novel multicellular human liver organoid model by co-culturing SB-HEO with HUVECs and LX-2 cells. This 3D system integrates hepatocytes, endothelial cells, and hepatic stellate cells, closely mimicking the cellular composition and structural characteristics of native human liver tissue. By applying TGF-β stimulation for 48 h, we successfully established a robust human liver fibrosis model based on 3hlLOs and further performed phenotypic screening of anti-fibrotic compounds. We identified AS191, a novel aspirin derivative, as a potent anti-fibrotic candidate with prominent therapeutic effects in vitro. The protective efficacy of AS191 against liver fibrosis was further validated in a CCl_4-induced

murine fibrotic model. Mechanistically, combined functional experiments and multi-omics analyses demonstrated that AS191 alleviates hepatic fibrosis progression by negatively regulating the PI3K/AKT signaling pathway.

2 Materials and methods

2.1 Cell Culture

Hepatic organoids (SB-HEO) were differentiated from human induced pluripotent stem cells (hiPSCs; Cellapy Biotechnology, China) according to previously described protocols[15]. LX-2 hepatic stellate cells (Procell Life Science & Technology, CL-0560) were cultured in high-glucose DMEM (Gibco, C11995500BT) supplemented with 10% fetal bovine serum (Gibco, 10091148) and 1% penicillin–streptomycin (Gibco, 15140122). Human umbilical vein endothelial cells (HUVECs; Procell Life Science & Technology, CM-0675) were maintained in ECM complete medium (ScienCell, 1001). All cell lines used in this study were legally sourced and authenticated by their respective vendors. All cells were cultured in a humidified incubator at 37°C with 5% CO_2.

2.2 Generation of 3hlLOs

To establish the co-culture system, we referred to published literature and finally adopted a 1:1 mixture of hepatic organoid medium and HUVEC medium, supplemented with 5% Matrigel (MCE, HY-K6004). For the experiment, SB-HEOs, HUVECs and LX-2 cells were mixed at a ratio of 4:2:1, and seeded into U-bottom ultra-low attachment 96-well plates (Corning, 7007) at a density of 2×10^5 cells per well. The plates were centrifuged at 300 g for 3 min using a horizontal centrifuge and incubated overnight. Three days later, the medium was replaced with mixed medium containing 3 μM CHIR99021, 5 μM Forskolin, 100 ng/mL VEGF and 50 ng/mL FGF2 for subsequent culture. Hepatic spheroid organoids were generated after 16 days of incubation.

2.3 CCl_4-Induced Hepatic Fibrosis in Mice

The design, execution, and reporting of all animal experiments in this study adhere to the Animal Research: Reporting of In Vivo Experiments (ARRIVE) guidelines 2.0. Male C57BL/6J mice (6 weeks old, 18–20 g, SPF grade) were purchased from Beijing Huafukang Bioscience Co., Ltd. (Beijing, China, certificate No. SCXK (Jing) 2024-0003). Animals were housed in a temperature-controlled environment (19–23°C) with ad libitum access to standard chow and water, under a 12-hour light/dark cycle. A total of 23 mice were used in this study.

A total of 23 male C57BL/6 mice were randomly divided into four groups (n = 5, 6, 6, 6): Control, Model, Colchicine (0.1 mg/kg), and AS191 (304 mg/kg). The AS191 dose was determined based on the clinical dosage of aspirin for anti-inflammatory and anti-rheumatic indications in humans, with 304 mg/kg serving as the murine equivalent. Except for the Control group, which received daily intraperitoneal (i.p.) injections of an equivalent volume of olive oil, all other groups were administered CCl_4 dissolved in olive oil (volume ratio 1:4) via i.p. injection once daily for 28 consecutive days to induce hepatic fibrosis. Drug

interventions began concurrently with modeling and continued throughout the 28-day period to evaluate the effect of AS191 on liver fibrosis. All mice had free access to food and water during the experiment. At the end of the treatment period, mice were fasted for 12–24 hours. Blood samples were collected via retro-orbital bleeding. After clotting at room temperature for 1 hour, serum was separated by centrifugation at 4°C and 1006 × g for 15 minutes, aliquoted, and stored at − 80°C until further analysis. Immediately after blood collection, mice were euthanized by cervical dislocation. Liver tissues were rapidly excised, rinsed with ice-cold physiological saline to remove residual blood and non-hepatic tissue, blotted dry, snap-frozen in liquid nitrogen, and subsequently stored at − 80°C for downstream experiments.

All animal procedures were conducted in strict accordance with the guidelines approved by the Institutional Animal Care and Use Committee (IACUC) of Tianjin Tiancheng New Drug Evaluation Co., Ltd. (Ethics Approval No.: PD-2026-02). At the endpoint, mice were anaesthetised with isoflurane (3% induction, 1.5–2% maintenance in 100% oxygen) via inhalation. Blood was collected via retro-orbital bleeding under deep anaesthesia. Mice were then euthanised by cervical dislocation.

2.4 Bulk RNA-seq data processing and analysis

For bulk RNA-seq data analysis, raw sequencing reads were subjected to quality control using fastp (v0.23.1) to remove adapter sequences and low-quality reads. The trimmed reads were aligned to the human reference genome (GRCh38/hg38) using STAR aligner (v2.7.8a), Gene annotation and quantification were performed based on GENCODE V35. Differential gene expression analysis between sample groups was conducted using the edgeR R package (v3.42.4). Genes with a false discovery rate (FDR) < 0.05 and an absolute fold change > 2 were defined as differentially expressed genes (DEGs). Gene Ontology (GO) and Kyoto Encyclopedia of Genes and Genomes (KEGG) pathway enrichment analyses of DEGs were conducted using the clusterProfiler R package.

2.5 Single-cell RNA sequencing library construction

The cell suspension was loaded into Chromium microfluidic chips with 3' v3 chemistry and barcoded with a 10x Chromium Controller (10x Genomics). RNA from the barcoded cells was subsequently reverse-transcribed and sequencing libraries constructed with reagents from a Chromium Single Cell 3' v3 reagent kit (10x Genomics) according to the manufacturer's instructions. Sequencing was performed with Illumina (NovaSeq) according to the manufacturer's instructions (Illumina, USA).

2.6 Single-cell RNA-seq data processing and analysis

For scRNA-seq analysis, raw sequencing data (FASTQ files) were processed using Cell Ranger (v5.0.1) with default parameters. Reads were aligned to the human reference genome (GRCh38), and gene expression matrices were generated for downstream analysis. All subsequent analyses were performed using the Seurat (v5.0.1) R package. To ensure data quality, key quality control (QC) metrics were evaluated for each sample, including the number of detected genes per cell (nFeature_RNA), total unique molecular identifier (UMI) counts per cell (nCount_RNA), and the percentage of mitochondrial gene

transcripts (percent.mt). Based on the distribution patterns observed in sample-specific QC violin and scatter plots, dynamic sample-specific filtering thresholds were applied to exclude low-quality cells, potential cell debris, and cells with excessive mitochondrial content indicative of compromised cell integrity. Potential doublets were identified and removed using DoubletFinder (v2.0.6) for each sample independently.

The filtered gene expression matrices were normalized using the "LogNormalize" method implemented in the NormalizeData function. The top 2000 highly variable genes were identified using the FindVariableFeatures function with the "vst" selection method. Normalized expression data were then scaled and centered using the ScaleData function. Principal component analysis (PCA) was performed based on the identified highly variable genes. Unsupervised cell clustering was conducted using graph-based methods via the FindNeighbors and FindClusters functions. Dimensionality reduction and visualization were performed using Uniform Manifold Approximation and Projection (UMAP).

Cell type annotation was performed based on the expression of canonical marker genes and cluster-specific differentially expressed genes identified using the FindAllMarkers function with default parameters. Gene ontology enrichment analysis was performed using the clusterProfiler R package.

For integration analysis, scRNA-seq data from publicly available liver tissue samples (GEO accession: GSE115469) were downloaded and integrated with our organoid datasets using Seurat integration workflow. Specifically, integration anchors were identified using the FindIntegrationAnchors function, and datasets were integrated using the IntegrateData function to correct for batch effects. Following integration, standard data scaling, dimensionality reduction and clustering were performed on the integrated dataset to enable cross-dataset comparisons.

2.7 H&E staining

The harvested organoids were fixed in 4% paraformaldehyde (PFA, Solarbio, China) for 30 min at room temperature (RT). After fixation, samples were resuspended in 3% agarose solution, solidified on ice, and subsequently processed through dehydration, paraffin embedding, and serial sectioning at a thickness of 3 μm. For histological observation, sections were deparaffinized, rehydrated, and subjected to routine hematoxylin and eosin (H&E) staining.

2.8 Immunofluorescence staining

Whole liver organoids were fixed with 4% PFA for 1 hour at room temperature, followed by three washes with PBST. After permeabilization with Triton X-100 for 30 minutes, the samples were blocked with 5% BSA for 1 hour at room temperature. After blocking, the organoids were placed at 4°C and incubated with primary antibodies against COL1A1 (Cell Signaling Technology, 72026), COL3A1 (Cell Signaling Technology, 63034), Desmin (Cell Signaling Technology, 5332), α-SMA (Cell Signaling Technology, 19245), CD31 (Cell Signaling Technology, 3528), PDGFRβ (Cell Signaling Technology, 3169), p-PI3K, p-AKT, and p-GSK-3β for 48 h. After thorough washing with PBST, the samples were incubated at 4°C in the dark with Alexa Fluor® 488 (Abcam, ab150113) and Alexa Fluor® 594 (Abcam, ab150080) fluorescent

secondary antibodies for an additional 48 h. Finally, the cell nuclei were counterstained with DAPI (Abcam, ab104139). All fluorescence images were acquired using a Leica TIRF & Thunder microscope (Leica, Germany).

2.9 Spheroid exposure to TGF-β

To induce hepatic fibrosis in 3hlLOs, organoids were treated with 25 ng/mL TGF-β (Novoprotein, CA59) for 48 h beginning on culture day 14. Organoids treated with an equal volume of 1% bovine serum albumin (BSA, MCE, HY-D0842A) served as the vehicle control. Six independent parallel organoids from each group were harvested for total RNA extraction.

2.10 Flow cytometric analysis

3hlLOs were dissociated into single-cell suspensions using TrypLE solution and resuspended in staining buffer. For flow cytometric analysis of surface and intracellular phosphorylated proteins, cells were fixed, permeabilized, and incubated with primary antibodies against CD140b (BD Biosciences, 558821), p-PI3K (Cell Signaling Technology, 12217-1-AP), p-AKT (Cell Signaling Technology, MA5-14891), and p-GSK-3β (Cell Signaling Technology, 5558). After primary antibody incubation, cells were stained with Alexa Fluor® 594 (Cell Signaling Technology, 8889). Cell fluorescence signals were acquired using a BD FACSCalibur flow cytometer, and raw data were further analyzed with FlowJo software.

2.11 Immunoblotting

Protein samples were analysed using the following antibodies: TGF-βR1 (Cell Signaling Technology, 49728), TGF-β (Abcam, ab66043), SMAD2/3 (Cell Signaling Technology, 8685), p-GSK-3β (Cell Signaling Technology, 5558), p-PI3K (Proteintech, 12217-1-AP), p-AKT (Thermo Fisher, MA5-14891), AKT (Cell Signaling Technology, 9272), GAPDH (Proteintech, 60004-1-Ig), HRP-conjugated Goat Anti-Mouse IgG (Proteintech, SA00001-1), and HRP- conjugated Goat Anti-Rabbit IgG (Proteintech, SA00001-2).

2.12 RNA extraction and qRT-PCR

Total RNA was extracted using the TransZol Up Plus RNA Kit (Transgen, ER501-01-V2). cDNA was synthesised with the Transcriptor First Strand cDNA Synthesis Kit (Roche) on a T100 Thermal Cycler (BIO-RAD). Quantitative PCR (qPCR) was performed using FastStart Universal SYBR Green Master (ROX) (Roche) on the Roche LightCycler 480 II Real-Time System. Data were normalised to GAPDH, and fold changes relative to the control group were calculated using the $2-\Delta\Delta CT$ method.

The following primers were used:

GAPDH-F: AGCCACATCGCTCAGACAC

GAPDH-R: GCCCAATACGACCAAATCC

COL1A1-F: GACACAGAGGTTTCAGTGG

COL1A1-R: CACCCTTAGCACCAACAG

ACTA2-F: CTGTTCCAGCCATCCTTCAT

ACTA2-R: TCATGATGCTGTTGTAGGTGG

LOXL2-F: CACAGTTGTCATCAACATTACC

LOXL2-R: CTGACCTTTAGGATATAGTTTCCAG

SLCO1B1-F: GCAATAGCAATGATTGGTCC

SLCO1B1-R: CCAACCCATCGAGAATCAG

GSTA1-F: CTGCCCGTATGTCCACCTG

GSTA1-R: AGCTCCTCGACGTAGTAGAGA.

2.13 Statistical analysis

All statistical analyses were performed using GraphPad Prism (version 8.3.0) and R software (version 3.6.2). Data were presented as the mean ± standard error of the mean (SEM). Single comparisons between two independent datasets were performed using an unpaired Student's t-test. Multiple comparisons across one variable were carried out using a one-way analysis of variance (ANOVA). Statistical significance was defined as follows: *P < 0.05, **P < 0.01, ***P < 0.001, ****P < 0.0001, ns indicates no significant difference.

3 Results

3.1 Generation and characterization of a coculture model of 3hlLOs

Hepatic stellate cell activation is the core initiating event that drives the onset and progression of hepatic fibrosis[16]. The establishment of liver organoid models with high hepatic maturation and multilineage biomimetic characteristics is critical for elucidating the pathological mechanisms of hepatic fibrosis and achieving precise screening of anti-fibrotic drugs[17]. Conventional liver organoids derived from single hepatocyte lineages exhibit insufficient maturation, simplified cellular composition, and a lack of vascular and stromal microenvironments, which limits their capacity to faithfully recapitulate the complex pathological processes of human hepatic fibrosis[18].

Accordingly, referring to well-established experimental systems for constructing vascularized human liver tissues and culturing multilineage hepatic and biliary organoids[19, 20], we determined the optimal coculture ratio of 4:2:1 for SB-HEOs, HUVECs, and LX-2 cells based on the synergistic growth characteristics of hepatocytes, vascular endothelial cells, and hepatic stellate cells. To promote the ordered aggregation, differentiation and functional maturation of organoids, pulsed WNT signaling

activation induced by CHIR99021 was applied to facilitate efficient cell assembly, and Forskolin was supplemented to enhance hepatic functional differentiation and further promote the maturation of 3hlLOs[21]. In addition, to reconstruct the hepatic vascular microarchitecture, 3hlLOs were cultured in medium containing VEGF165 and FGF2 for 8 consecutive days to generate mature 3hlLOs with intact structure and stable function. The detailed experimental procedure is illustrated in Fig. 1A. Bright-field microscopic observation showed that SB-HEOs, HUVECs, and LX-2 cells efficiently aggregated and assembled into uniform, compact, smooth-edged three-dimensional organoid spheroids with favorable morphological integrity in the optimized coculture system (Fig. 1B). Detection of key functional genes demonstrated that the expression levels of hepatocyte-specific markers *SLCO1B1* and *GSTA1* were continuously upregulated during culture, indicating progressive differentiation and functional maturation of hepatocytes inside 3hlLOs. Meanwhile, the expression of hepatic stellate cell signature genes including *COL1A1*, *LOXL2* and *ACTA2* remained stable in the middle and late stages of culture without abnormal upregulation or excessive cellular activation. This result indicated that LX-2 cells were maintained in a quiescent state without spontaneous fibrotic activation, which meets the fundamental requirements for subsequent fibrosis induction experiments (Fig. 1C).

To further characterize the viability, engraftment efficiency and homeostatic properties of LX-2 cells within the co-culture system, flow cytometry was used to quantitatively detect the expression of the hepatic stellate cell-specific marker PDGFRβ (Fig. 1D). The results showed that LX-2 cells stably resided within the 3D architecture of 3hlLOs, and their proportion exhibited a mild yet steady upward trend throughout the culture period. These findings verified that the optimized cell ratio and culture conditions could effectively sustain the viability, proliferative capacity and biological activity of LX-2 cells, and support the synergistic and stable growth of multiple hepatic cell lineages. Furthermore, immunofluorescence staining confirmed the multi-lineage cellular composition of 3hlLOs, which stably expressed core cell markers, including ALB, CD31, α-SMA and PDGFRβ (Fig. 1E). H&E staining verified that mature 3hlLOs possessed homogeneous internal structures and distinct tissue layers without obvious apoptosis or central necrosis, demonstrating that this culture system supports long-term survival and stable growth of organoids (Fig. 1F). Collectively, the successfully established 3hlLOs display typical hallmarks of hepatic maturation and recapitulate the complex cellular heterogeneity of native liver tissues.

3.2 Single-cell transcriptome analysis of 3hlLOs

To characterize the cellular composition and intrinsic properties of 3hlLOs after multilineage coculture, we performed single-cell transcriptomic profiling. Single-cell RNA sequencing (scRNA-seq) was utilized to dissect the cellular heterogeneity of mature 3hlLOs. Cluster analysis resolved a total of 10 distinct cell clusters based on global gene expression patterns (Fig. 2A). According to canonical lineage-specific biomarkers, these clusters were further annotated into three major cell lineages: hepatobiliary, mesenchymal, and endothelial populations (Fig. 2B). Quantitative composition analysis demonstrated that 3hlLOs were composed of 65.86% endothelial cells, 30.86% hepatobiliary cells, and 3.27% mesenchymal cells (Fig. 2C). Lineage-specific signature genes exhibited high cell-type specificity and

were exclusively enriched in their corresponding cell populations, confirming accurate cellular classification (Fig. 2D, 2E). Gene Ontology enrichment analysis of lineage-specific differentially expressed genes revealed divergent functional features among the three cell subtypes. Genes upregulated in the mesenchymal lineage were primarily enriched in mitochondrial energy metabolism and protein biosynthesis pathways. Endothelial lineage-enriched DEGs were mainly associated with cell cycle progression, cell proliferation, and cell division. In contrast, genes highly expressed in the hepatobiliary lineage were functionally linked to hepatic metabolic homeostasis and liver immune regulation (Fig. 2F). To evaluate the transcriptional similarity between 3hlLOs and native human liver tissue, we integrated our scRNA-seq data with a public human liver single-cell dataset. UMAP visualization showed that 3hlLO-derived hepatocytes clustered closely with primary human liver cells, indicating high transcriptional similarity to in vivo liver cells (Fig. 2G). To further assess the transcriptional maturation level of our engineered organoids, we performed transcription factor enrichment analysis among iPSCs, SB-HEOs, 3hlLOs, and primary human hepatocytes (PHHs). The results revealed that 3hlLOs acquired more mature transcriptional networks governing hepatic immune homeostasis and epithelial differentiation compared with SB-HEOs (Fig. 2H). To determine whether 3hlLOs are suitable for hepatic fibrosis modeling, we compared the transcriptomic differences between SB-HEOs and 3hlLOs through hierarchical clustering and GO functional enrichment. The DEGs heatmap showed that multiple key pro-fibrotic genes, including TWIST1, COL3A1, and IL6, were significantly upregulated in 3hlLOs (Fig. 2I). Consistently, GO enrichment further verified that mesenchymal proliferation and stromal activation pathways were uniquely enriched in multilineage 3hlLOs (Fig. 2J). Since hepatic fibrosis progression is tightly dependent on aberrant progenitor proliferation, excessive epithelial–mesenchymal transition, and dynamic parenchymal–mesenchymal crosstalk, the inherent mesenchymal-endothelial-hepatobiliary multilineage constitution endows 3hlLOs with greater sensitivity to fibrotic stimuli such as TGF-β. Therefore, 3hlLOs can faithfully recapitulate core fibrotic events, including extracellular matrix accumulation and EMT activation. In summary, the engineered 3hlLOs exhibit superior hepatic maturation, complex tissue-like cellular heterogeneity, and inherent pro-fibrotic responsiveness, thus providing a robust and reliable platform for in vitro hepatic fibrosis modeling and mechanistic research.

3.3 Phenotypic analysis of liver fibrosis models established by TGF-β-induced 3hlLOs

Transforming growth factor-β is a canonical pro-fibrotic cytokine that serves as a central inducer of hepatic fibrosis under various pathological liver conditions[22]. To evaluate the capacity of 3hlLOs for in vitro fibrotic modeling, we treated mature 3hlLOs with 25 ng/mL TGF-β for 48 h and subsequently characterized the pathological phenotypes (Fig. 3A). Morphological observations revealed that the compact and intact spheroid structure of 3hlLOs became loose and disorganized following TGF-β stimulation (Fig. 3B). ATP activity assays further demonstrated that TGF-β treatment markedly reduced the overall cellular viability of 3hlLOs (Fig. 3C). qPCR analysis confirmed that the mRNA levels of core fibrotic markers, including COL1A1, ACTA2, and LOXL2, were substantially upregulated in TGF-β-exposed

3hlLOs compared with untreated controls (Fig. 3D). Consistent with these findings, Calcein-AM/PI double staining showed a significant increase in cell death in the TGF-β-treated group, indicating obvious hepatocellular injury induced by fibrotic stimulation (Fig. 3E). Flow cytometric quantification further revealed an increased proportion of CD140b-positive cells, which represents activated hepatic stellate cell populations, after TGF-β intervention (Fig. 3F). Moreover, comprehensive immunofluorescence staining validated that TGF-β stimulation significantly promoted extracellular secretion of type I collagen and elevated the protein expression of multiple fibrotic biomarkers, including COL1A1, COL3A1, DESMIN, and α-SMA (Fig. 3G, 3H). Collectively, these results demonstrate that 3hlLOs can robustly respond to TGF-β stimulation and recapitulate key pathological features of hepatic fibrosis, including cellular injury, stellate cell activation, and extracellular matrix deposition, thereby supporting the reliability and applicability of 3hlLOs as a versatile in vitro platform for hepatic fibrosis modeling.

3.4 Sequencing analysis of TGF-β-induced 3hlLOs recapitulating liver fibrosis

To systematically investigate the alterations in cellular composition and intrinsic characteristics of 3hlLOs following TGF-β stimulation (designated T-3hlLOs), we performed single cell RNA sequencing transcriptomic profiling of fibrotic organoids. Cluster analysis of global gene expression profiles identified nine distinct cell clusters in T-3hlLOs (Fig. 4A), which were further annotated and classified into six well defined cell types based on lineage specific gene expression patterns (Fig. 4B). Quantitative cellular composition analysis revealed that T-3hlLOs consisted of 26.7% hepatic progenitor cells, 1.16% mature hepatocytes, 1.48% stressed epithelial cells, 20.16% cholangiocytes, 47.83% endothelial cells, and 2.67% activated fibroblasts (Fig. 4C). To verify the pathological similarity of our fibrotic model with clinical fibrotic liver tissues, we integrated the scRNA seq data of T-3hlLOs with a published single cell transcriptomic dataset of human cirrhotic liver tissues. UMAP dimensionality reduction analysis demonstrated that hepatocytes derived from T-3hlLOs clustered closely with primary hepatocytes from cirrhotic patient samples, indicating a high degree of transcriptional similarity to clinical fibrotic liver lesions (Fig. 4D). KEGG pathway enrichment heatmap analysis showed that T-3hlLOs exhibited significant enrichment of activated fibroblasts and robust upregulation of pro fibrotic signaling pathways, whereas metabolic pathways specific to mature hepatocytes were markedly suppressed, suggesting impaired hepatic metabolic function in TGF-β induced fibrotic organoids (Fig. 4E). Principal component analysis revealed a clear transcriptional separation between untreated 3hlLOs and TGF-β stimulated T-3hlLOs, confirming the effective and global transcriptomic reprogramming induced by TGF-β intervention (Fig. 4F). Differential gene expression analysis further demonstrated that TGF-β stimulation triggered widespread transcriptional repression in 3hlLOs, accompanied by specific upregulation of a panel of fibrosis related genes (Fig. 4G). Consistent with these findings, genes associated with phase I/II metabolic enzymes were collectively downregulated in T-3hlLOs, the bile acid synthesis, transport, and regulation networks were significantly suppressed, and hepatic glucose metabolism was also impaired. These results demonstrate that TGF-β treatment caused significant damage to liver organoids (Fig. 4H). Collectively, these transcriptomic alterations strongly validate that

TGF-β stimulation can reliably induce stable fibrotic phenotypes in 3hlLOs, enabling the successful construction of an in vitro hepatic fibrosis model. Finally, KEGG pathway enrichment analysis was performed to explore the key signaling pathways involved in TGF-β mediated hepatic fibrosis. The results indicated that the top significantly enriched pathways included the immunoglobulin superfamily cell adhesion molecule (IgSF CAM) pathway, nonalcoholic fatty liver disease (NAFLD) pathway, bile secretion pathway, p53 signaling pathway, and multi species apoptosis pathway (Fig. 4I).

3.5 Screening of anti-fibrotic compounds based on 3hlLOs

Liver fibrosis is a wound-healing response to stimuli that cause liver damage[23]. When the triggering factors persist, liver fibrosis can progress to cirrhosis, which may further develop into liver cancer or liver failure; currently, there are no effective treatments[24]. Therefore, we established a liver fibrosis model based on 3hlLOs to screen for anti-fibrotic drugs. Our complete workflow is shown in Fig. 5A. In this study, we used the intensity of type I collagen immunofluorescence staining as a quantitative indicator of the degree of liver fibrosis to screen 138 candidate compounds with potential antifibrotic activity (Supplement table 1). The screening system included a blank solvent group, a TGF-β fibrosis model group, and a pirfenidone-positive control group as a triple control. Preliminary screening results showed that a total of 7 compounds significantly inhibited TGF-β-induced abnormal overexpression of COL1A1 (Fig. 5B). We further validated the inhibitory effects of these 7 compounds (AS191, Sunitinib, PIT-1, I3MT-3, Dovitinib, Masitinib, and Amuvatinib) on TGF-β-induced liver fibrosis using flow cytometry (Fig. 5C).

3.6 AS191 alleviates TGF-β–Induced Hepatic Fibrosis in 3hlLOs via regulating the PI3K/AKT signaling pathway

To further elucidate the molecular mechanism underlying the anti fibrotic activity of the screened compounds, we focused on the optimal candidate AS191 and systematically explored its regulatory signaling pathways in fibrotic liver organoids. To determine the optimal working concentration of AS191 in T-3hlLOs, we evaluated fibrotic severity based on COL1A1 immunofluorescence intensity. Gradient concentration treatment confirmed that 20 μM AS191 exerted the most potent anti fibrotic effect (Fig. 6A). It is well established that TGF-β signaling is divided into canonical Smad dependent and non canonical Smad independent pathways[25]. The canonical Smad cascade primarily mediates downstream transcriptional regulation, whereas the non canonical branch activates multiple secondary signaling cascades, including PI3K/AKT and MAPK pathways, to modulate cell survival, migration, and pathological progression[26]. To clarify the mechanism by which AS191 alleviates hepatic fibrosis, we first examined the activation status of the canonical TGF-β/Smad pathway. Western blot results showed that AS191 treatment significantly reduced the protein levels of TGF-β and TGFβR1 in T 3hlLOs, while the phosphorylation levels of Smad2/3 remained unchanged (Fig. 6B). These findings indicated that the anti fibrotic effect of AS191 was independent of the canonical Smad signaling pathway. We next investigated whether AS191 functioned through the non canonical PI3K/AKT cascade. Western blot analysis demonstrated that AS191 markedly inhibited the phosphorylation of PI3K, AKT, and its downstream

effector GSK3β (Fig. 6C). Consistently, flow cytometry and immunofluorescence staining further verified that AS191 effectively suppressed the hyperactivation of the PI3K/AKT signaling pathway (Fig. 6D, 6E). In summary, these results demonstrate that AS191 ameliorates hepatic fibrosis by blocking the TGF-β mediated non canonical PI3K/AKT signaling cascade, thereby inhibiting the progression of liver fibrotic pathology (Fig. 6F).

3.7 Network pharmacology and molecular docking reveal the core mechanism of AS191 against hepatic fibrosis

To systematically complement and interpret the above cellular-level findings, we further integrated network pharmacology and molecular docking technologies to decipher the potential molecular mechanism of AS191. First, based on the chemical structural characteristics of AS191 (Fig. 7A), potential drug targets were predicted and intersected with hepatic fibrosis-related disease targets. A total of 108 common targets that mediate the pharmacological activity of AS191 and are highly correlated with the pathological progression of hepatic fibrosis were identified (Fig. 7B). A protein-protein interaction (PPI) network was constructed for these intersecting targets, followed by topological analysis, from which nine key hub targets including ALB, AKT1 and STAT3 were screened out (Fig. 7C, 7D). Accumulating literature has validated that these molecules exert central regulatory functions throughout the initiation, progression and even regression of hepatic fibrosis.

To characterize the direct interaction between AS191 and core targets, six top-ranked hub targets in the PPI network (ALB, AKT1, ESR1, STAT3, EGFR, NF-κB) were selected for molecular docking simulation and verification (Fig. 7E, 7F). Docking results demonstrated that AS191 could form stable molecular binding conformations with high affinity to all tested core targets of hepatic fibrosis. KEGG pathway enrichment analysis revealed that the core signaling pathways modulated by AS191 were significantly enriched in canonical fibrosis-related cascades such as PI3K/AKT and MAPK signaling pathways (Fig. 7G). Further functional enrichment analysis indicated that biological process (BP) terms were mainly enriched in protein phosphorylation, signal transduction and positive regulation of apoptosis; cellular component (CC) terms were predominantly distributed in receptor complexes, extracellular regions and cytoplasm; molecular function (MF) terms were primarily associated with nuclear receptor activity, homologous protein binding and enzyme binding activity (Fig. 7H). Collectively, the above enrichment results provide theoretical evidence for deciphering the potential biological functions and molecular mechanism of AS191, and confirm that the PI3K/AKT signaling axis serves as the core regulatory pathway responsible for the anti-hepatic fibrosis pharmacological efficacy of AS191.

3.8 In vivo validation of anti-fibrotic activity and PI3K/AKT inhibitory mechanism of AS191 in CCl_4-induced hepatic fibrotic mice

To consolidate the above in vitro and bioinformatic conclusions, we further validated the anti-fibrotic efficacy and molecular mechanism of AS191 using a classic CCl_4-induced mouse hepatic fibrosis in vivo model. The detailed modeling procedure is illustrated in Fig. 8A. In vivo experimental results revealed

that AS191 treatment markedly reduced liver weight and liver coefficient in mice, alleviated hepatic inflammatory infiltration and collagen deposition, and restored the structural integrity of liver tissue (Fig. 8B–8D). Consistent with the histological observations, serum levels of alanine transaminase (ALT), aspartate transaminase (AST) and alkaline phosphatase (ALP) were significantly decreased in all AS191 administration groups, indicating obvious amelioration of liver function injury (Fig. 8E). Meanwhile, Western blot assays verified that AS191 effectively suppressed the aberrantly high expression of TGF-β and α-SMA in fibrotic liver tissues (Fig. 8F). Moreover, the phosphorylation levels of PI3K and AKT were prominently downregulated in liver tissues from AS191-treated mice (Fig. 8G).

In summary, multi-dimensional in vitro and in vivo experiments in this study collectively demonstrated that AS191 exerts potent anti-hepatic fibrosis effects by specifically inhibiting the non-canonical PI3K/AKT signaling pathway, thereby alleviating CCl_4-induced hepatocellular injury and pathological fibrotic progression.

4 Discussion

Induced pluripotent stem cell (iPSC)-derived functional liver organoids have shown great potential in disease modeling, drug screening, and regenerative medicine. Although multiple types of differentiated liver organoids can be obtained from iPSCs, most conventional models lack diverse non-parenchymal cells residing in native liver tissues, including hepatic stellate cells, endothelial cells, and immune cells[18, 27]. Accumulating studies have demonstrated that non-parenchymal cells are essential for maintaining hepatic physiological homeostasis and participate in the pathological progression of various liver diseases[28]. The crosstalk between parenchymal and non-parenchymal cells critically modulates liver function, injury response, and fibrotic progression[29]. Therefore, the construction of multicellular liver organoids that faithfully recapitulate endogenous cell interactions is essential for establishing precise in vitro liver disease models and exploring pathological mechanisms. To overcome the limitations of traditional single-lineage liver organoids and establish a reliable platform for fibrotic mechanism research and anti-fibrotic drug screening, we constructed an advanced multicellular liver organoid model by co-culturing SB-HEOs, HUVECs, and LX-2 cells. The established 3hlLOs possess complex structural characteristics and high cellular heterogeneity, effectively compensating for the insufficient pathological simulation capacity of conventional liver organoids. Using this biomimetic model, we successfully induced stable fibrotic phenotypes, performed compound screening, and identified AS191, an aspirin derivative, as a potent anti-fibrotic candidate. Furthermore, we systematically elucidated the molecular mechanism by which AS191 regulates transcriptional reprogramming and alleviates hepatic fibrosis.

SB-HEOs adopted in this study are self-assembled three-dimensional hepatic progenitor aggregates with excellent expandability and long-term genetic stability[15]. After continuous expansion, SB-HEOs maintain stable cystic structures, intact transcriptional profiles, and consistent differentiation potential toward mature hepatic progenitors, exhibiting physiological and transcriptomic characteristics highly similar to those of native liver tissues. Compared with conventional two-dimensional hepatic progenitor cultures,

SB-HEOs provide a superior tissue-like microenvironment and serve as a stable and renewable parenchymal cell source for constructing complex liver organoids. By co-culturing SB-HEOs with HUVECs and LX-2 cells, we achieved spontaneous cellular self-assembly and stable formation of mature 3hlLOs. On day 16 of culture, 3hlLOs exhibited compact and intact structures and stably expressed specific markers of hepatocytes, hepatic stellate cells, and endothelial cells, indicating stable maintenance of multilineage cellular composition. To fully characterize the biological features and functional advantages of 3hlLOs, we performed single-cell RNA sequencing and transcriptomic profiling. Functional enrichment analysis revealed that the upregulated genes in 3hlLOs were primarily involved in mitochondrial energy metabolism, protein biosynthesis, cell proliferation, hepatic metabolism, and immune responses. Compared with single-lineage liver organoids, 3hlLOs displayed significantly higher basal expression of inflammation and fibrosis related genes, thereby exhibiting higher sensitivity to fibrotic stimulation and enabling stable induction of fibrotic pathological phenotypes for long-term mechanistic investigation.

TGF-β is a pivotal pro-fibrotic cytokine that triggers hepatic stellate cell activation and excessive extracellular matrix deposition, serving as a core driving factor of chronic liver fibrosis[30]. In the present study, stable fibrotic organoid models were successfully established via continuous TGF-β stimulation[31]. TGF-β treatment disrupted the compact structure of 3hlLOs, reduced cellular ATP activity, and induced evident hepatocellular injury and pro-fibrotic alterations. Transcriptomic and single-cell analyses demonstrated that genes related to basal hepatic function and tissue homeostasis were markedly suppressed in T-3hlLOs, whereas pathways associated with fibrosis progression, extracellular matrix remodeling, and myofibroblast activation were significantly enriched. The transcriptional characteristics of T-3hlLOs are highly consistent with clinical fibrotic liver tissues, confirming that this model reliably recapitulates human hepatic fibrosis and is suitable for anti-fibrotic drug screening and mechanistic exploration. Using the validated T-3hlLOs fibrotic model, we conducted large-scale compound screening and identified AS191 as a promising anti-fibrotic candidate. Subsequent in vitro functional experiments further confirmed that the antifibrotic effect of AS191 does not depend on the classical TGF-β/Smad pathway, but rather specifically inhibits the non-classical PI3K/AKT signaling cascade, thereby blocking hepatic stellate cell activation and collagen deposition. This study combined network pharmacology and molecular docking techniques to predict the core targets of AS191, confirming its stable, high-affinity binding to key regulatory molecules involved in fibrosis; enrichment analysis further demonstrated that the PI3K/AKT pathway is the core signaling axis mediating the antifibrotic function of AS191. Finally, this study fully validated the therapeutic efficacy and molecular mechanism of AS191 in an in vivo CCl_4-induced mouse model of liver fibrosis: AS191 alleviates liver damage, inhibits pathological collagen accumulation, and downregulates PI3K/AKT pathway phosphorylation in animals.

Nevertheless, the current study has several limitations. First, the cellular composition of 3hlLOs does not fully recapitulate that of native human liver tissue. The relative abundance of endothelial cells is higher in 3hlLOs, whereas the proportion of mature hepatocytes remains limited, particularly under fibrotic

stimulation. This discrepancy may affect the generalizability of our findings to human liver pathophysiology. Second, the current 3hlLOs system lacks immune components such as Kupffer cells, which are critical for modulating liver inflammation and fibrotic progression. Third, the in vivo experiments were conducted with a relatively small sample size and a single animal model (CCl_4-induced fibrosis), which does not capture the heterogeneity of human liver fibrosis etiologies. Fourth, the treatment duration in the animal model was limited to 28 days; therefore, the long-term efficacy, safety, and potential adverse effects of AS191 remain to be evaluated. Fifth, although network pharmacology and molecular docking predicted PI3K/AKT as the core target of AS191, these in silico analyses are inherently predictive and require further validation through biochemical assays (e.g., kinase activity assays) and structural biology approaches. Sixth, the pharmacokinetic properties, bioavailability, and potential off-target effects of AS191 were not assessed in this study. Finally, all findings are derived from preclinical models, and the translational relevance to human patients requires rigorous clinical validation. Future studies will focus on optimizing the organoid culture system, incorporating additional hepatic cell lineages (e.g., Kupffer cells, biliary epithelial cells), and evaluating AS191 in more diverse fibrosis models and ultimately in clinical settings.

Nevertheless, the current study has several limitations. First, the cellular composition of 3hlLOs does not fully recapitulate that of native human liver tissue. The relative abundance of endothelial cells is higher in 3hlLOs, whereas the proportion of mature hepatocytes remains limited, particularly under fibrotic stimulation. This discrepancy may affect the generalizability of our findings to human liver pathophysiology. Second, the current 3hlLOs system lacks immune components such as Kupffer cells, which are critical for modulating liver inflammation and fibrotic progression[27]. Third, the in vivo experiments were conducted with a relatively small sample size and a single animal model (CCl_4-induced fibrosis), which does not capture the heterogeneity of human liver fibrosis etiologies. Fourth, the treatment duration in the animal model was limited to 28 days; therefore, the long-term efficacy, safety, and potential adverse effects of AS191 remain to be evaluated. Fifth, although network pharmacology and molecular docking predicted PI3K/AKT as the core target of AS191, these in silico analyses are inherently predictive and require further validation through biochemical assays and structural biology approaches. Sixth, the pharmacokinetic properties, bioavailability, and potential off-target effects of AS191 were not assessed in this study. Finally, all findings are derived from preclinical models, and the translational relevance to human patients requires rigorous clinical validation. Future studies will focus on optimizing the organoid culture system, incorporating additional hepatic cell lineages, and evaluating AS191 in more diverse fibrosis models and ultimately in clinical settings.

5 Conclusions

In conclusion, our study established a strategy for constructing biomimetic liver organoids via the co-culture of SB-HEOs, LX-2 cells, and HUVECs. Based on this well-characterized 3hlLOs platform, we successfully generated a stable fibrotic organoid model through TGF-β stimulation. Screening of antifibrotic compounds using the T-3hlLOs fibrotic model identified AS191 as a potential anti-fibrotic

candidate. Cross-validation results between in vitro organoid models and an in vivo mouse model of CCl_4-induced liver fibrosis consistently indicate that AS191 attenuates the pathological features of liver fibrosis and alleviates liver damage in preclinical settings. At the molecular level, functional experiments conducted both in vitro and in vivo suggest that AS191 primarily exerts its hepatoprotective and anti-fibrotic effects by downregulating the non-canonical PI3K/AKT signaling pathway, thereby attenuating the progression of fibrosis. However, further preclinical and clinical studies are warranted to validate the therapeutic potential of AS191 in human liver fibrosis.

Declarations

Acknowledgements

We gratefully acknowledge the financial support provided by State Key Laboratory of Druggability Evaluation and Systematic Translational Medicine, Project of Science and Technology Program of Tianjin, CAMS Innovation Fund for Medical Sciences for the completion of this research.

Authors' contributions

WYC: Conceptualization, Methodology, Data curation, Formal Analysis, Writing Original Draft. SL: Conceptualization, Methodology, Validation. LBW: Conceptualization, Data Curation, Software, Validation. ZZL: Conceptualization, Investigation. PTY and XLZ and TYZ: Formal analysis. XLW: Project administration. ZW: Project administration, Conceptualization, Writing Review & Editing. All authors have read and approved the final manuscript.

Ethics approval and consent to participate

Procedures of animal experimental were recognized by Institutional Animal Care and Use Committee (IACUC) committee at Tianjin Institute of Pharmaceutical Research (TIPR), in compliance with "Guide for the Care and Use of Laboratory Animals" (National Research Council of the USA, 1996) and the relevant ethical regulations of China Academy of Chinese Medical Sciences. This animal experiment project was approved under the project number CYZH-B2025019-02-02, with the ethical approval number PD-2026-02. All animal procedures were reviewed and approved by the Animal Ethics Committee of Tianjin Tiancheng New Drug Evaluation Co., Ltd.

We confirm that this study adheres to the ARRIVE guidelines for reporting animal research. Following the completion of the experiment, mice were euthanized via cervical dislocation under anesthesia.

Funding

Project of Science and Technology Program of Tianjin (25ZXZSSS00940, 24ZXZSSS00480, 62524ZYCGSY00640), State Key Laboratory of Druggability Evaluation and Systematic Translational Medicine (712025011-1-2, 712025011-2-2, and 712025011-2-3).

Declaration of AI use

The authors confirm that no generative artificial intelligence or AI-assisted technologies were used in the preparation of this manuscript.

Competing interests

The authors declare that they have no competing interests.

Consent for publication

Not applicable.

References

1. H. Ayabe, T. Anada, T. Kamoya, et al., Optimal Hypoxia Regulates Human iPSC-Derived Liver Bud Differentiation through Intercellular TGFB Signaling, Stem cell reports, 11 (2018) 306-16.
2. S. Ariño, R. Ferrer-Lorente, G. Serrano, et al., Patient-derived liver organoids recapitulate liver epithelial heterogeneity and enable precision modeling of alcohol-related liver disease, Journal of hepatology, 84 (2026) 135-49.
3. S.K. Asrani, J. Mellinger, J.P. Arab, et al., Reducing the Global Burden of Alcohol-Associated Liver Disease: A Blueprint for Action, Hepatology (Baltimore, Md.), 73 (2021) 2039-50.
4. J.P. Thiery, H. Acloque, R.Y.J. Huang, et al., Epithelial-Mesenchymal Transitions in Development and Disease, Cell, 139 (2009) 871-90.
5. G.M. Balachander, I.C. Ng, R.R. Pai, et al., LEADS - a comprehensive human liver-on-a-chip for non-alcoholic steatohepatitis (NASH) drug testing, Lab on a chip, 25 (2025) 3444-66.
6. Y. Shi, Y. Zhang, D. Liu, et al., Diosgenin alleviates hepatic fibrosis via PI3K/Akt/mTOR mediated fatty acid metabolic reprogramming and NF-κB activation, Journal of Ethnopharmacology, 367 (2026).
7. C.C. Bell, D.F. Hendriks, S.M. Moro, et al., Characterization of primary human hepatocyte spheroids as a model system for drug-induced liver injury, liver function and disease, Scientific reports, 6 (2016) 25187.
8. J.M. Llovet, R. Pinyol, S. Affo, et al., Hallmarks of liver cancer: Therapeutic implications, Cell, 189 (2026) 2490-514.
9. S. Bartfeld, H. Clevers, Organoids as Model for Infectious Diseases: Culture of Human and Murine Stomach Organoids and Microinjection of Helicobacter Pylori, Journal of visualized experiments : JoVE, (2015).
10. Y. Zhang, Y. Liu, X. Wu, et al., Prophylactic systemic low-dose pirfenidone attenuates intrauterine adhesion by inhibiting the TGF-β1/Smad3 pathway, Biochimica et Biophysica Acta (BBA) - Molecular Basis of Disease, 1872 (2026).

11. Y. Xin, G. Chen, M.M. Hammour, et al., Three-Dimensional Human Liver Micro Organoids and Bone Co-Culture Mimics Alcohol-Induced BMP Dysregulation and Bone Remodeling Defects, Cells, 15 (2026).
12. A.I. Ardisasmita, I.F. Schene, I.P. Joore, et al., A comprehensive transcriptomic comparison of hepatocyte model systems improves selection of models for experimental use, Communications Biology, 5 (2022).
13. C. Olgasi, A. Cucci, A. Follenzi, iPSC-Derived Liver Organoids: A Journey from Drug Screening, to Disease Modeling, Arriving to Regenerative Medicine, International Journal of Molecular Sciences, 21 (2020).
14. H. Zhang, P.N. Thai, R.V. Shivnaraine, et al., Multiscale drug screening for cardiac fibrosis identifies MD2 as a therapeutic target, Cell, 187 (2024) 7143-63.e22.
15. S. Liu, Z. Wang, L. Zhu, et al., Generation and applications of an expandable and mature hiPSC-derived liver organoid, Acta Pharmaceutica Sinica B, 15 (2025) 6382-98.
16. Y. Yoon, S.C. Gong, M.Y. Kim, et al., Generation of Fibrotic Liver Organoids Using Hepatocytes, Primary Liver Sinusoidal Endothelial Cells, Hepatic Stellate Cells, and Macrophages, Cells, 12 (2023).
17. O. Sirenko, M.K. Hancock, J. Hesley, et al., Phenotypic Characterization of Toxic Compound Effects on Liver Spheroids Derived from iPSC Using Confocal Imaging and Three-Dimensional Image Analysis, ASSAY and Drug Development Technologies, 14 (2016) 381-94.
18. L. Cools, M.K. Dastjerd, A. Smout, et al., Human iPSC-derived liver co-culture spheroids to model liver fibrosis, Biofabrication, 16 (2024).
19. Y. Miao, N.M. Pek, C. Tan, et al., Co-development of mesoderm and endoderm enables organotypic vascularization in lung and gut organoids, Cell, 188 (2025) 4295-313.e27.
20. T. Takebe, K. Sekine, M. Enomura, et al., Vascularized and functional human liver from an iPSC-derived organ bud transplant, Nature, 499 (2013) 481-84.
21. K.Y. Chi, G. Kim, H. Kim, et al., Optimization of culture conditions to generate vascularized multi-lineage liver organoids with structural complexity and functionality, Biomaterials, 314 (2025).
22. B. Dewidar, C. Meyer, S. Dooley, et al., TGF-β in Hepatic Stellate Cell Activation and Liver Fibrogenesis—Updated 2019, Cells, 8 (2019).
23. J. Lotto, T.L. Stephan, P.A. Hoodless, Fetal liver development and implications for liver disease pathogenesis, Nature Reviews Gastroenterology & Hepatology, 20 (2023) 561-81.
24. H.J. Kim, G. Kim, K.Y. Chi, et al., Generation of multilineage liver organoids with luminal vasculature and bile ducts from human pluripotent stem cells via modulation of Notch signaling, Stem Cell Research & Therapy, 14 (2023).
25. X.H. Chen, L.l. Lu, H.P. Ke, et al., The TGF-β-induced up-regulation of NKG2DLs requires AKT/GSK-3β-mediated stabilization of SP1, Journal of Cellular and Molecular Medicine, 21 (2017) 860-70.
26. J. Massagué, D. Sheppard, TGF-β signaling in health and disease, Cell, 186 (2023) 4007-37.

27. S.P. Harrison, R. Siller, Y. Tanaka, et al., Scalable production of tissue-like vascularized liver organoids from human PSCs, Experimental & Molecular Medicine, 55 (2023) 2005-24.
28. Y. Li, Y. Nie, X. Yang, et al., Integration of Kupffer cells into human iPSC-derived liver organoids for modeling liver dysfunction in sepsis, Cell Reports, 43 (2024).
29. J. Lee, D. Gil, H. Park, et al., A multicellular liver organoid model for investigating hepatitis C virus infection and nonalcoholic fatty liver disease progression, Hepatology, 80 (2024) 186-201.
30. L. Huang, C. Zhang, L. Su, et al., GSK3β attenuates TGF-β1 induced epithelial–mesenchymal transition and metabolic alterations in ARPE-19 cells, Biochemical and Biophysical Research Communications, 486 (2017) 744-51.
31. M.V. Plikus, X. Wang, S. Sinha, et al., Fibroblasts: Origins, definitions, and functions in health and disease, Cell, 184 (2021) 3852-72.

Figures

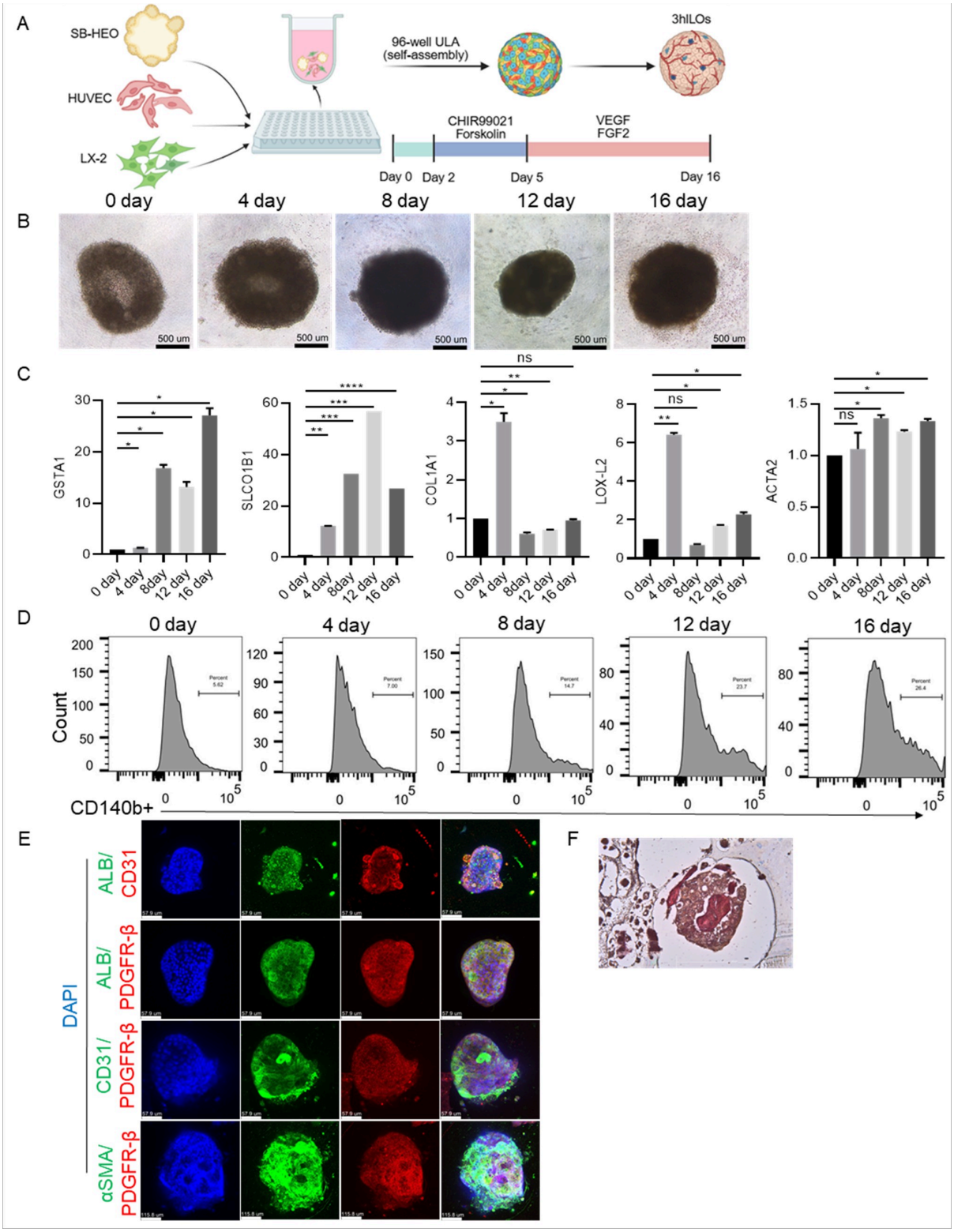


Figure 1

Characterization of the multi-lineage hepatic organoid (3hlLOs). (A) Schematic illustration of the construction strategy of 3hlLOs. Created with BioRender.com. (B) Bright-field morphological observation of 3hlLOs during the 16-day culture period. (C) qRT-PCR analysis of hepatocyte functional genes (*GSTA1*, *SLCO1B1*) and hepatic stellate cell characteristic genes (*COL1A1*, *LOXL2*, *ACTA2*) in 3hlLOs on day 16 of culture. (D) Flow cytometric detection of the dynamic changes in the positive proportion of the hepatic

stellate cell marker CD140b during 3hlLOs culture. (E) Whole-mount immunofluorescence staining of 3hlLOs on day 16 of culture. (F) H&E staining of 3hlLOs on day 16 of culture.

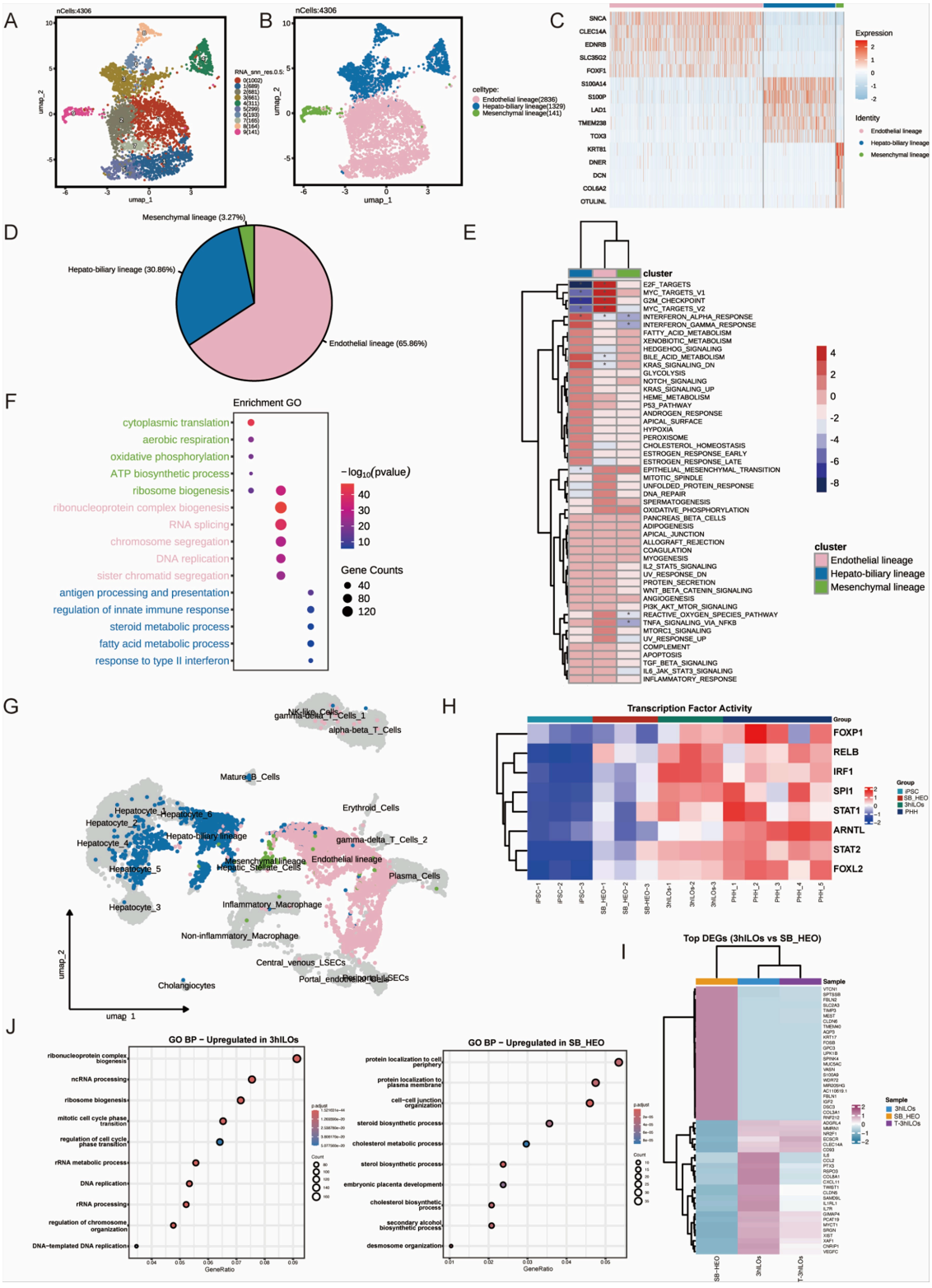


Figure 2

Sequencing and bioinformatic analysis of 3hlLOs. (A) Cell clustering distribution of 3hlLOs. (B) Cell type annotation of 3hlLOs based on the expression patterns of lineage-specific markers. (C) Expression

profiles of representative cell-type-specific markers. (D) Cellular component proportion of each cell cluster in 3hlLOs. (E) KEGG pathway enrichment analysis of differentially expressed genes in distinct cell clusters. (F) GO functional enrichment analysis of biological processes for each cell cluster. (G) Specific distribution characteristics of different cell types in 3hlLOs. (H) Activity profiles of the top eight human liver-specific transcription factors among iPSCs, SB-HEOs, 3hlLOs, and PHHs. (I) Heatmap analysis of differentially expressed genes between SB-HEOs and 3hlLOs. (J) GO biological process enrichment analysis of DEGs between SB-HEOs and 3hlLOs.

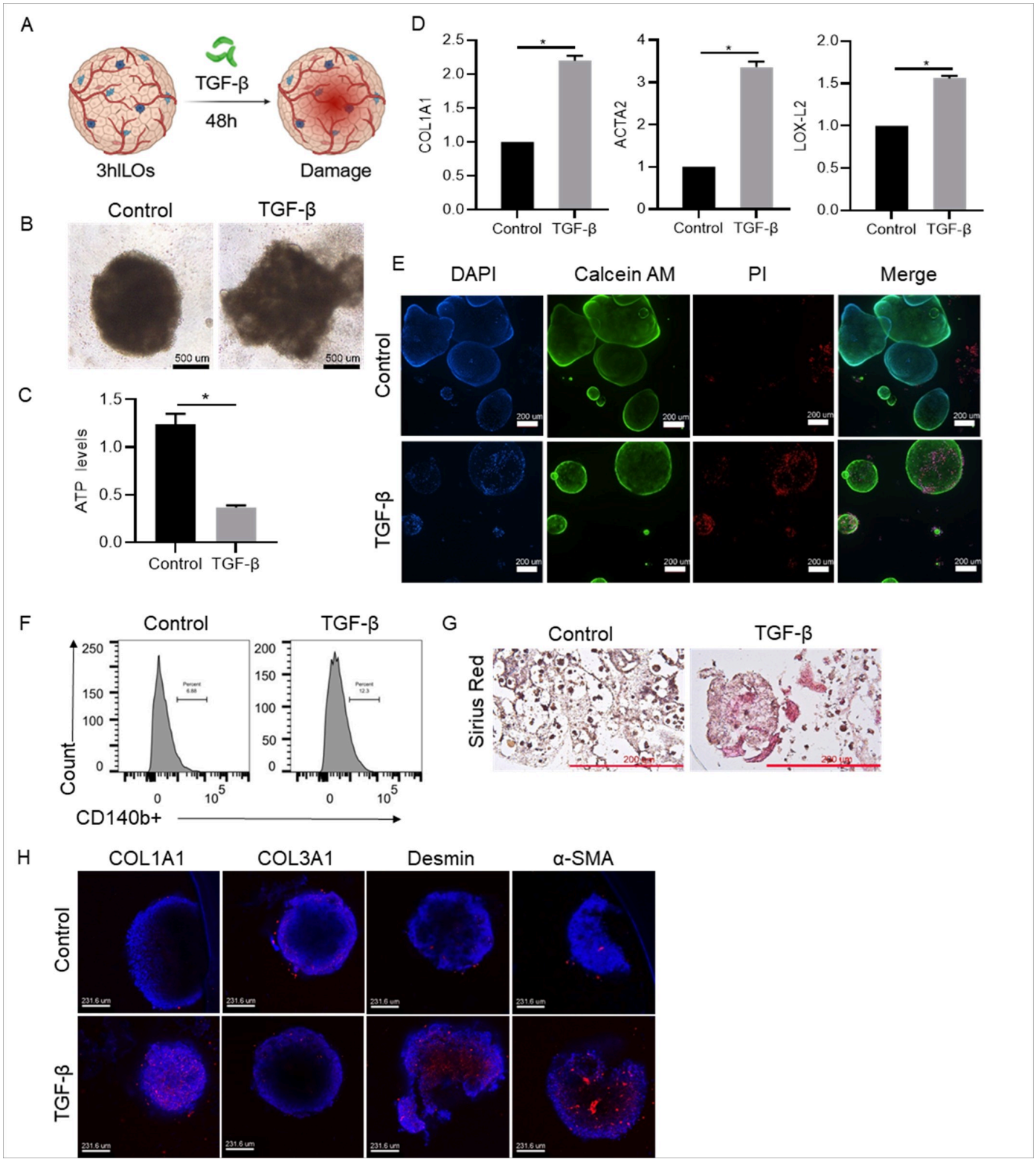


Figure 3

Phenotypic analysis of hepatic fibrosis modeled in the 3hlLOs system. (A) Schematic illustration of 3hlLOs after 48 h of TGF-β stimulation. Created with BioRender.com. (B) Bright field images of 3hlLOs after 48 h of TGF-β stimulation to activate hepatic stellate cells. (C) Cellular ATP activity of 3hlLOs after 48 h of TGF-β stimulation (n = 6 hepatic spheroids per group). (D) Relative mRNA expression levels of fibrosis related genes in 3hlLOs with or without 48 h TGF-β treatment (n = 6 hepatic spheroids per group). (E) Cell viability evaluation of 3hlLOs before and after TGF-β induction using Calcein AM/PI staining. (F) Flow cytometric analysis of the proportion of CD140b positive cells in 3hlLOs following 48 h TGF-β treatment. (G) Sirius Red staining of 3hlLOs after 48 h of TGF-β treatment. (H) Immunofluorescence staining of fibrosis associated proteins in TGF-β treated 3hlLOs.

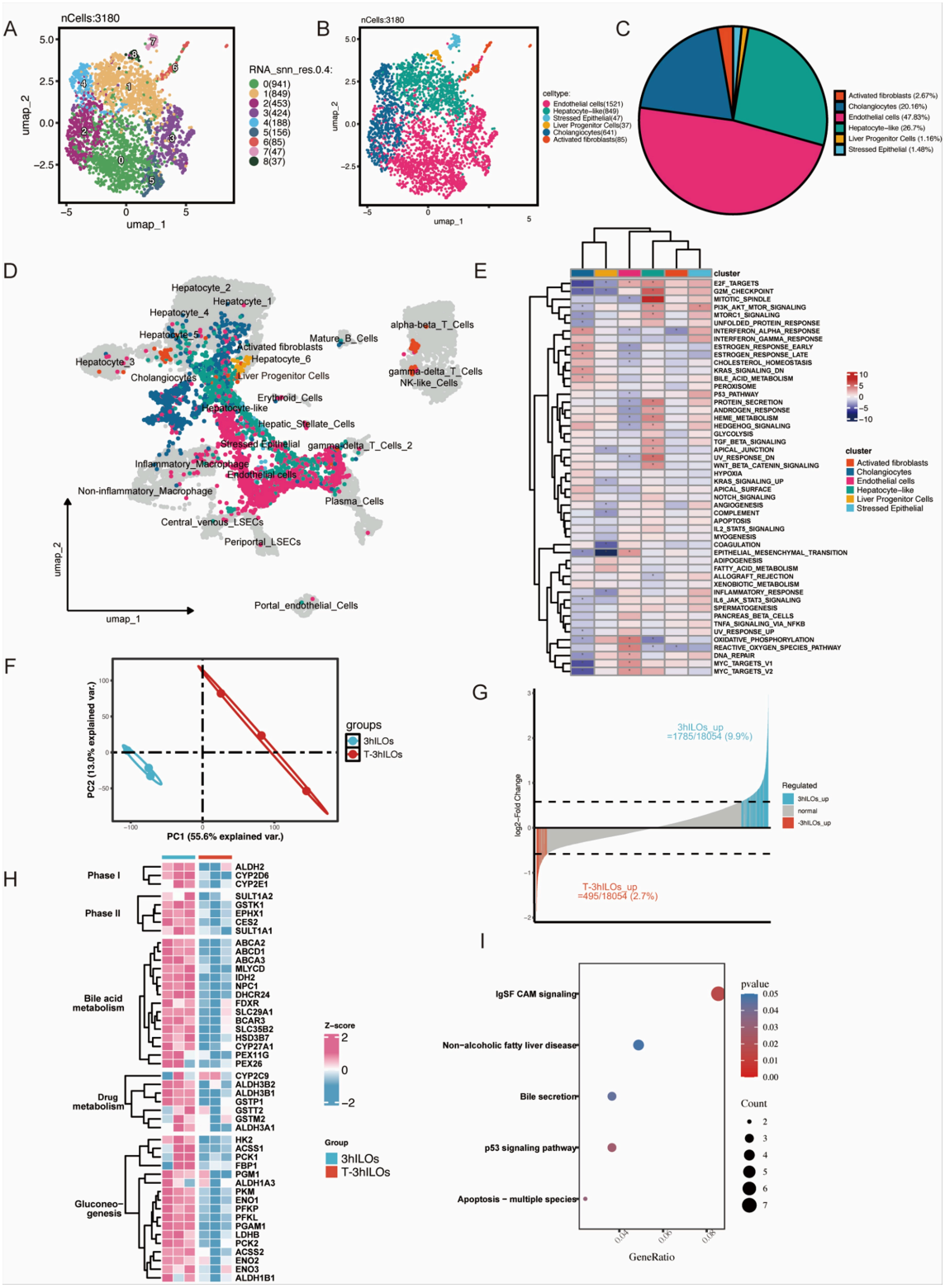


Figure 4

Identification of cellular composition and characteristics of T-3hILOs. (A) Cell clustering distribution of T-3hILOs. (B) Cell type annotation of T-3hILOs based on the expression patterns of lineage-specific markers. (C) Cellular component proportion of each cell cluster in T-3hILOs. (D) Cell-type-specific distribution of T-3hILOs. (E) Canonical signaling pathway enrichment analysis of distinct cell clusters in T-3hILOs. (F) PCA analysis of transcriptional profiles between 3hILOs and T-3hILOs. (G) Volcano plot of

DEGs between 3hlLOs and T-3hlLOs, showing a total of 495 genes significantly regulated by TGF-β stimulation. (H) Heatmap of differentially up- and downregulated genes in 3hlLOs and T-3hlLOs. (I) Bubble plot of KEGG pathway enrichment analysis for DEGs identified in T-3hlLOs.

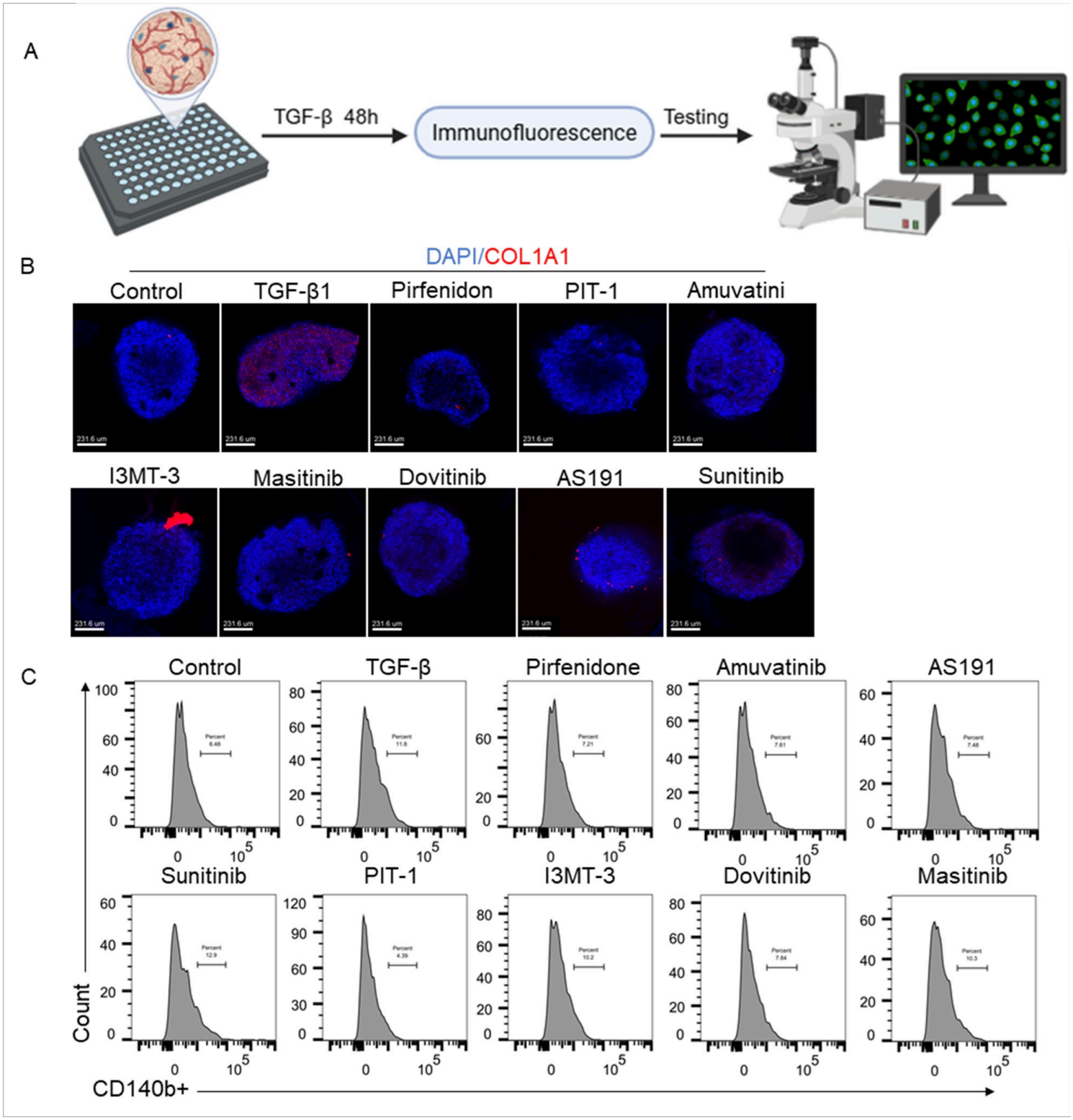


Figure 5

Drug screening based on the hepatic fibrosis organoid model. (A) Schematic workflow of drug screening using the T-3hlLOs fibrotic organoid model. Created with BioRender.com. (B) Immunofluorescence staining of the fibrotic marker COL1A1. (C) Flow cytometric analysis of the proportion of CD140b-positive hepatic stellate cells.

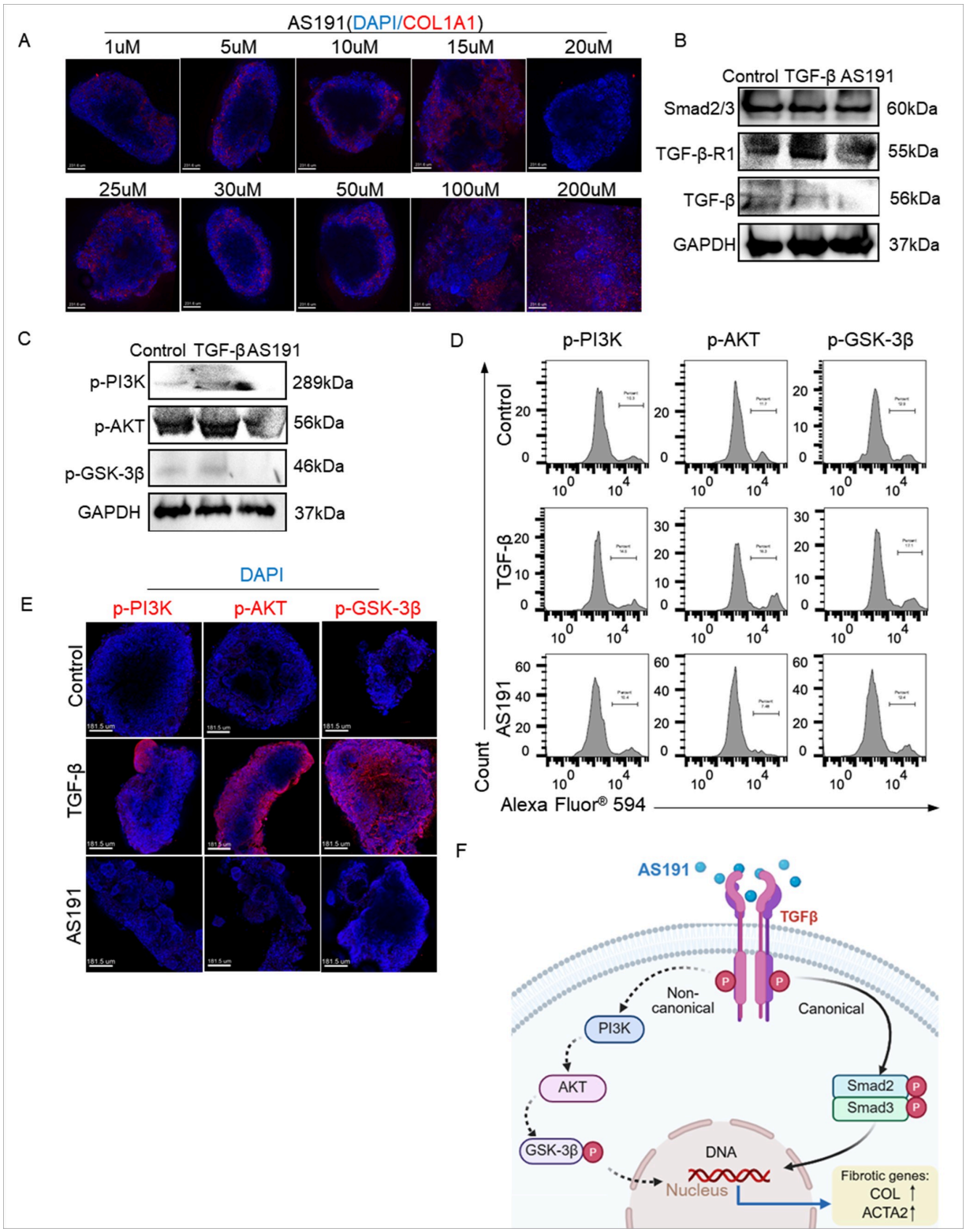
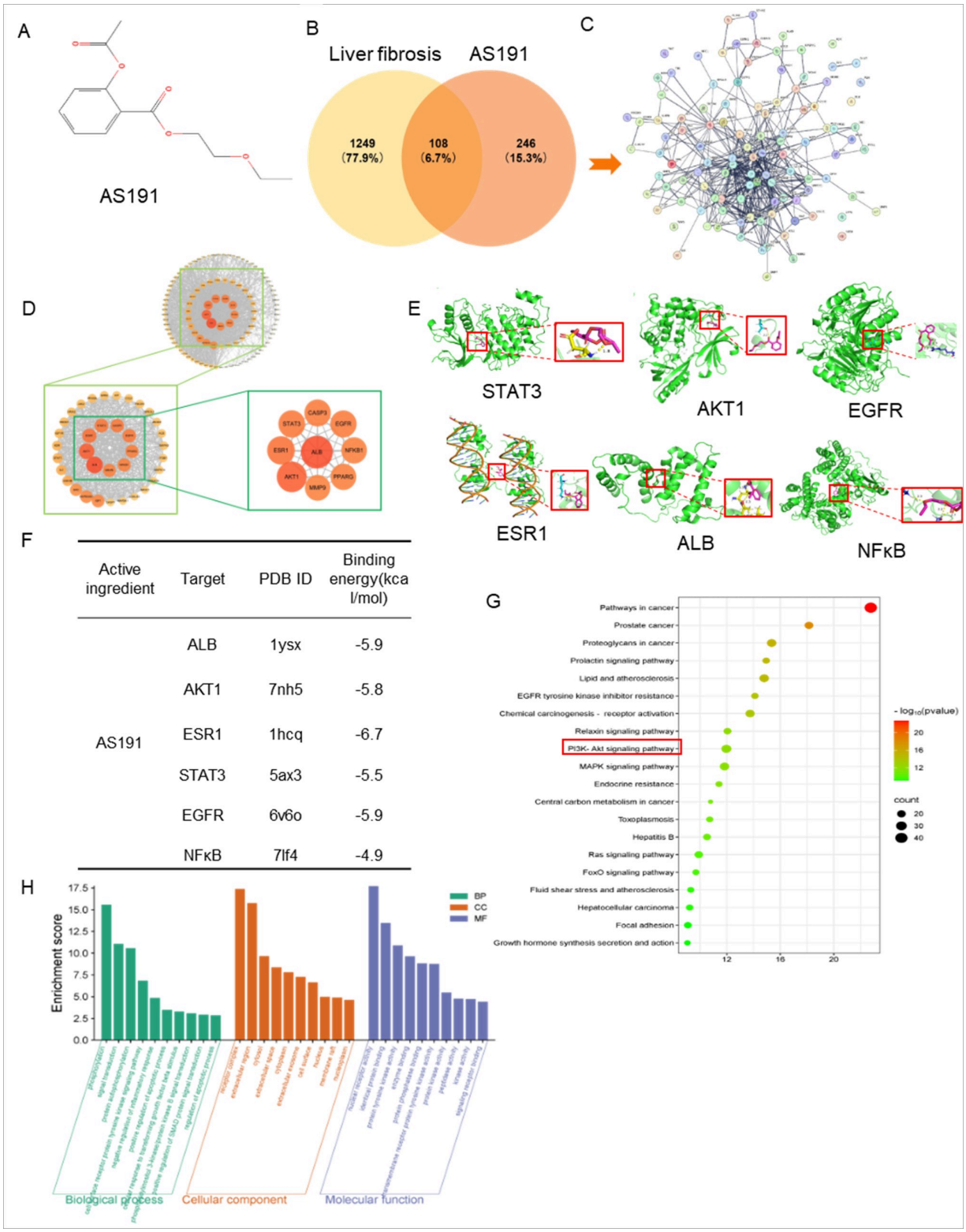


Figure 6

Mechanistic investigation of the anti-fibrotic signaling pathway regulated by AS191. (A) Immunofluorescence staining showing the optimal anti-fibrotic concentration of AS191. (B) Western blot results demonstrated that the anti-fibrotic effect of AS191 was independent of the canonical TGF-β/Smad2/3 signaling pathway. (C) Western blot results showing the regulation of the PI3K/AKT signaling pathway by AS191. (D) Flow cytometry analysis results of AS191 on the PI3K/AKT pathway and its downstream signaling molecules. (E) Immunofluorescence analyses results of AS191 on the PI3K/AKT pathway and its downstream signaling molecules. (F) Schematic diagram illustrating the molecular mechanism by which AS191 regulates hepatic fibrosis. Created with BioRender.com.



Active ingredient	Target	PDB ID	Binding energy(kcal/mol)
AS191	ALB	1ysx	-5.9
	AKT1	7nh5	-5.8
	ESR1	1hcq	-6.7
	STAT3	5ax3	-5.5
	EGFR	6v6o	-5.9
	NFκB	7lf4	-4.9

Figure 7

Bioinformatic prediction and molecular docking validation of AS191 against hepatic fibrosis. (A) The chemical structural characteristics of AS191. (B) Venn plot of AS191 and hepatic fibrosis targets. (C) PPI network of overlapping targets. (D) Topological hub gene screening. (E) 3D binding conformations of AS191 with six core targets. (F) Binding energy statistics of molecular docking. (G) KEGG pathway

enrichment bubble chart highlighting PI3K/AKT signaling. (H) GO enrichment bar graph for BP, CC and MF categories.

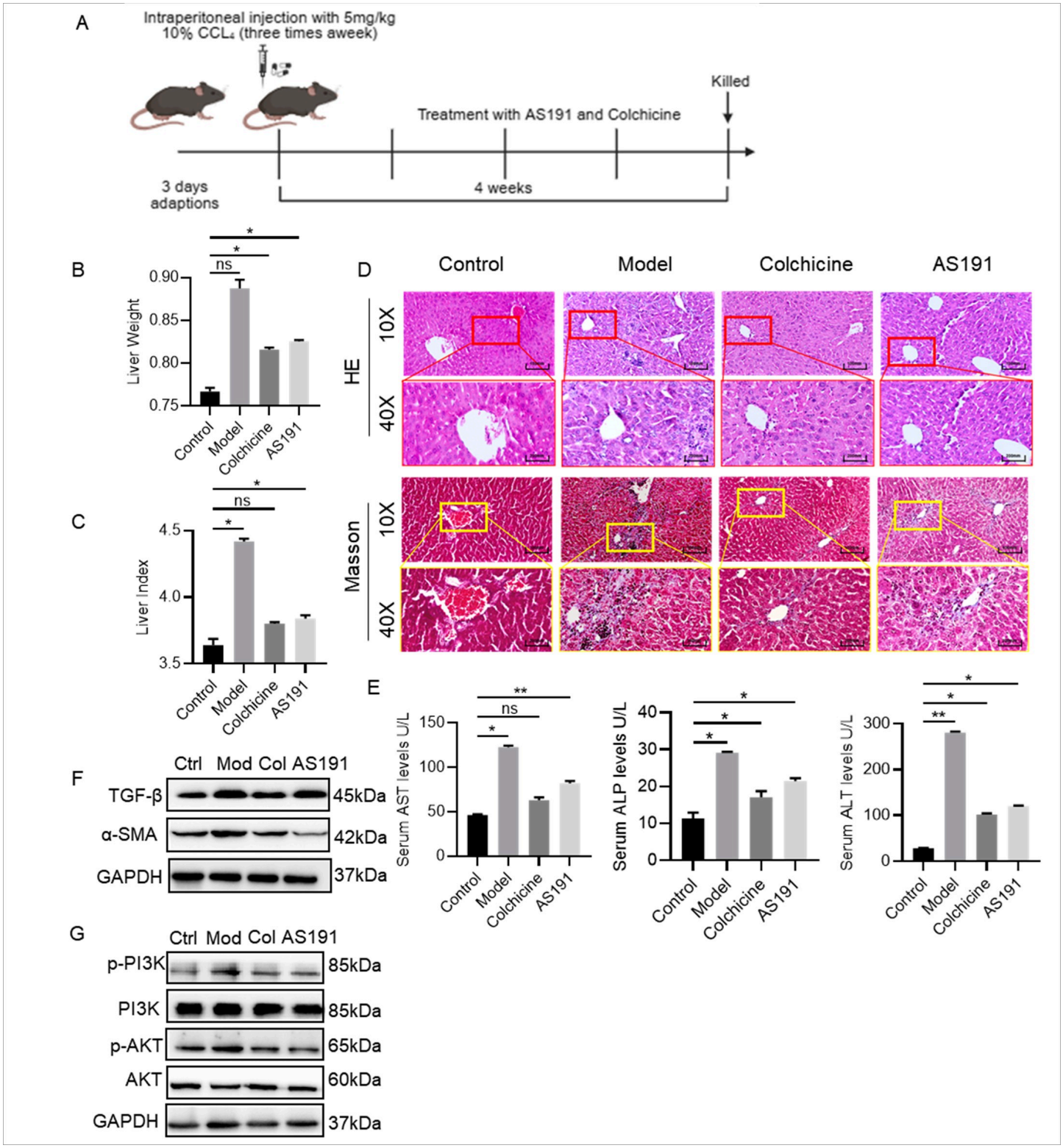


Figure 8

AS191 exerts anti-hepatic fibrosis effects and suppresses the PI3K/AKT signaling pathway in CCl_4-induced fibrotic mice. (A) Schematic diagram of the establishment of CCl_4-induced hepatic fibrosis

mouse model and drug intervention schedule. Created with BioRender.com. (B-C) Quantitative statistics of liver weight and liver index of mice in each group. (D) Representative images of H&E staining and Masson staining of liver tissues (10× and 20× magnification). (E) Quantitative detection of serum liver function markers ALT, AST and ALP. (F) Western blot analysis of the expression of fibrotic markers TGF-β and α-SMA in liver tissues. (G) Western blot detection of phosphorylated and total protein levels of PI3K/AKT signaling pathway in liver tissues.

Supplementary Files

This is a list of supplementary files associated with this preprint. Click to download.

- supplementtable1.docx
- AuthorChecklistFull.pdf
- SupplementaryUncroppedBlots.docx